




Investigating the correlation between the Urbach energy and asymmetry parameter of the Raman mode in semiconductors

Omkar V. Rambadey , Anil Kumar , and Pankaj R. Sagdeo ^{*}

Materials Research Laboratory, Department of Physics, Indian Institute of Technology Indore, Indore 453552, India

 (Received 9 August 2021; revised 15 November 2021; accepted 30 November 2021; published 16 December 2021)

A quantitative correlation between the Urbach energy (E_u) and asymmetry parameter q of Raman spectra has been derived. For this purpose, the effect of electronic disorder ($\sim E_u$) on the possible interference between the electronic continuum states and discrete phononic states is reinvestigated. The equation of the form $\frac{I}{q^2} \propto \xi E_u \pm \lambda$ (I : intensity of phonon mode ; ξ, λ : some material-dependent parameters) has been obtained and verified experimentally on different semiconductors. The experimental results reveal an offset which has been understood as intrinsic or disorder-induced contribution to electron-phonon interactions in the system. The obtained equations quantitatively explain the changes in the Raman line shape due to disorder induced by atomic substitutions, temperature, etc., and provide understanding of the superposition between electronic and phononic states and of electron-phonon coupling in semiconductors with disorder.

DOI: [10.1103/PhysRevB.104.245205](https://doi.org/10.1103/PhysRevB.104.245205)

I. INTRODUCTION

The exponential behavior of the optical absorption coefficient with incident photon energy near absorption edges, i.e., the behavior of Urbach tail states and the asymmetry parameter of the Raman phonon mode are believed to be of common origin, i.e., due to the electron-lattice coupling [1,2] The electron-lattice interaction is one of the fundamental interactions of quasiparticles in solids, which plays a crucial role for a variety of physical phenomena, such as superconductivity [3–5], colossal magnetoresistance [6–9], transport and thermodynamic properties [10], etc. Bloch [11] derived the electron-lattice matrix element for electrons in metals of the following form [12]:

$$g_{mnv}(\mathbf{k}, \mathbf{Q}) = -i \left(\frac{\hbar}{2N_P M_{\mathbf{k}} \omega_{\mathbf{Q}v}} \right)^{\frac{1}{2}} \mathbf{Q} \cdot \mathbf{e}_{\mathbf{k}v}(\mathbf{Q}) V_0.$$

The above equation considers the mass ($M_{\mathbf{k}}$) of ions, polarization of acoustic wave $\mathbf{e}_{\mathbf{k}v}(\mathbf{Q})$ corresponding to the wave vector \mathbf{Q} for various modes, and effective potential (V_0) experienced by electrons in the unit cell. This equation essentially represents the scattering of electrons in a metallic system due to acoustic phonons and neglected so called *umklapp* processes. The said effective potential experienced by electrons was then further improved by Nordheim [13], Mott and Jones [14], Bardeen [15], Nakajima [16], and Bardeen and Pines [17]. These efforts finally resulted in description of an electron-lattice mechanism using the field theoretical approach. Presently, in theory, the electron-phonon coupling (EPC) strength is estimated using the Eliashberg spectral function [5] $\lambda(\omega^2) = \int_0^\infty \alpha^2 F(\omega) \frac{d\omega}{\omega}$; where, $\alpha^2 F(\omega)$ describes an effective electron-electron interaction due to any type of boson exchange [18] (phonon, in solids).

In semiconductors, the charge carriers are generally confined within a narrow range in energy near the band edges; hence, the electron-lattice scattering mechanisms will be dominated by long-wavelength phonons ($\mathbf{k} \rightarrow 0$; \mathbf{k} = momentum vector). This was proposed by Bardeen and Shockley [19]. In this approach, the long-wavelength acoustic waves are used to describe the atomic displacements and later related to the elastic strain in the unit cell, which further leads to the deformation of the unit cell potential. It is well known that, due to (1) random distribution of crystallographic defects, (2) random distribution of impurities/doping and also due to external perturbations such as (3) temperature and (4) pressure, etc., potential fluctuations may be introduced into the system [20–23], which can give rise to the energy levels within the forbidden energy gap, also called *band tails* or *Urbach tail states* near band edges [23–25]. Due to the presence of these tail states near band edges, the charge carriers in semiconductors are no longer confined within the narrow energy range (as compared with that of disorder-free semiconductor materials) but in slightly broader energy range; hence, it is expected that the electron-lattice scattering mechanism will also have contribution from phonons with \mathbf{k} slightly > 0 , i.e., due to the non-zone-center phonons [26], which may lead to enhanced electron-lattice coupling [12,23]. Numerous theoretical and experimental efforts have been attempted to understand the electron-lattice coupling [27–31]; among various models, the theoretical models on EPC by Chamberlain *et al.* [32] and Cardona *et al.* [33] have been successfully applied to pure and doped semiconductor materials.

The EPC in semiconductors and its correlation with disorder has been one of the most challenging problems of condensed matter physics [34–37]. This problem is considered indirectly by introducing strain followed by first-principles calculations [38] and also by investigating dephasing or relaxation of electrons/phonons due to disorder [39]. Here, disorder is described as a product of characteristic momentum

^{*}Corresponding author: prs@iiti.ac.in

transfer due to EPC and mean free path because of scattering from impurities [39]; hence, the problem is treated similar to a metallike system. Further, in the case of semiconductors and insulators, the prediction of electron-lattice coupling using the GW approximation is found to be successful [40] but computationally very expensive and verified only for limited numbers of semiconductors, considering simplified crystal structures.

Experimentally, many research groups have employed various intriguing techniques to estimate the strength of electron-lattice coupling. Recently, Benedek *et al.* [41] reported a study of electron-lattice interaction in low-dimensional and layered structures by an He-atom scattering (HAS) experiment. In their work, subsurface phonons were detected on multilayer metallic structures via the HAS technique. Moreover, the angle-resolved photoemission spectroscopy (ARPES) technique has also been known as a tool to estimate the coupling strength [42]. Na *et al.* [43] employed the ARPES technique in the time domain for the graphite system to study electron-lattice interactions. Additionally, Raman spectroscopy [44–49] and optical spectroscopy [5,24,50] are useful nondestructive techniques to qualitatively probe EPC in semiconductors. Raman spectroscopy has been widely used for qualitative understanding of EPC [1,32,51] by analyzing the Raman line shape in terms of asymmetry [47,52,53] and antiresonance peaks [1,54,55], where the Fano resonance [55] is employed to model EPC. The line shape asymmetry/antiresonance is addressed by the asymmetry parameter q , the inverse of which is proportional to the strength of coupling [45,50,56]. The Fano model considers the interaction between the continuum and discrete states, deducing the dependence of q on the width of this interaction band [55]. However, while assuming its application in Raman spectroscopy, no direct expression accounting for the effect of disorder on EPC has been reported. It is noteworthy that any structural or chemical influences in the lattice can affect the electronic as well as phononic band structures as a consequence of induced disorders [57,58]; in the energy scale, the phononic spread due to such a structural disorder is predicated to be small (per a few centimeters) [59–61]; hence, the phonon spread could also be expected to contribute in the electron-lattice interaction in the system and the information of the phonon spread, i.e., the full width at half maximum (FWHM) of the phonon mode, is already inbuilt in the Fano asymmetric parameter q [51,55]. Moreover, semiconductors at finite temperatures exhibit structural disorder [58]; these disorders result in additional states near the valence band (VB) and/or conduction band (CB), known as Urbach tail states [24,62,63], being a measure of electronic disorder arising mainly due to structural, thermal, or chemical disorders and are experimentally probed as the Urbach energy (E_u) [64], which generally spreads over a few millielectronvolts to 100 meV [47,58,65,66]. The E_u has significant importance in determining the optoelectronic and photovoltaic properties of materials [66,67]. Also, the origin of E_u is understood in terms of interaction of excitons and phonons in the system [68]. Therefore, there appears a possible correlation of E_u with the interaction of charge carriers and lattice vibrations [24].

Keeping this in view here, the Fröhlich Hamiltonian is divided into pure and disorder-containing terms in the Fano

model, yielding a quantitative relationship between EPC in the form of asymmetry parameter q estimated from Raman spectroscopy and electronic disorder measured in terms of the Urbach energy (E_u) extracted from optical absorption spectroscopy (OAS) that has the form $I/q^2 \propto E_u$ (I being the intensity of Raman mode exhibiting asymmetry), which is further experimentally supported for Hf-doped BaTiO₃, temperature-varied TiO₂, and Si single-crystal samples, revealing enhancement in coupling-strength ($\sim 1/q$) with electronic disorder ($\sim E_u$). In addition, the obtained mathematical equations completely explain the changes in the Raman line shape as a function of disorder. This strategy could be applicable to almost all types of semiconductors and provides accurate information of EPC as a function of disorder using Raman and optical spectroscopy.

II. EXPERIMENTAL DETAILS

A. Sample details

Commercially available anatase TiO₂ powder (Alfa Aesar with purity 99.999%) and a silicon single-crystal (111) sample were used for the analysis. Synthesis of Hf-incorporated barium titanate BaTi_(1-x)Hf_xO₃ (BTHO) was carried out with the solid-state route for various compositions. The detailed discussion on sample preparation and the x-ray diffraction analysis for the present series of samples were reported in previous work [47,58].

B. Experimental techniques

1. Optical/Urbach energy measurements

The optical measurements of prepared samples were performed using diffuse reflectance spectroscopy on an ultraviolet-visible-near infrared spectrophotometer [69–74].

2. Raman spectroscopy

The Raman measurements were performed on the samples using a high-resolution dispersive spectrometer equipped with a 633 nm excitation laser source and a charge-coupled device detector in backscattered mode [75–77].

III. THEORETICAL DISCUSSIONS AND BACKGROUND

To establish the relation between electronic disorder and electron-lattice coupling for disordered systems, we consider a discrete phononic state and a continuum of electronic states, and to theoretically correlate the experimentally obtained results, the mathematical treatment by Fano [55] will be followed. Let $|\rho\rangle$ represent a discrete phononic state with energy eigenvalue E_ρ . Then [55]

$$\langle \rho | \hat{H} | \rho \rangle = E_\rho, \quad (1.1)$$

and $|\varkappa\rangle$, a continuum of electronic states with energy eigenvalues E_\varkappa , and the elements of the part of the energy matrix belonging to the subset of states $|\rho\rangle$ and $|\varkappa\rangle$ would form a square submatrix which, after diagonalization, can be written as [55]

$$\langle \varkappa | \hat{H} | \rho \rangle = V_{\varkappa\rho}. \quad (1.2)$$

To constrain the discussion to one continuum of states, consider the orthogonality between other continuum states $|\mathcal{X}'\rangle$ which may be present in the system [55]:

$$\langle \mathcal{X}' | \hat{H} | \mathcal{X} \rangle = E_{\mathcal{X}} \delta(E_{\mathcal{X}'} - E_{\mathcal{X}}). \quad (1.3)$$

To account for the effects of EPC, the corresponding Fröhlich Hamiltonian \hat{H} is given by

$$\hat{H} = \hat{H}_e + \hat{H}_\rho + \hat{H}_{e\rho}. \quad (1.4)$$

Here, \hat{H}_e includes the coulombic interactions in an ideally periodic lattice; \hat{H}_ρ denotes the quantized harmonic lattice vibrations or noninteracting phonons; and the term $\hat{H}_{e\rho}$ describes the coupling between the electrons and phonons. For samples having structural disorder due to strain, defects, impurity, etc., such disorders are known to produce electronic disorder in the form of Urbach tail states, also termed as the Urbach energy [24,25,67,78]. As a result of which, the term \hat{H}_e could be expressed as $\hat{H}_e = \hat{H}_e^0 + \hat{H}_e^d$, where the additional term \hat{H}_e^d accounts for the fluctuation in the coulombic potential due to the structural disorder induced by defects, doping, temperature, pressure, etc. Also, the term $\hat{H}_{e\rho}$ in Eq. (1.4) can be expressed as $\hat{H}_{e\rho} = \hat{H}_{e\rho}^0 + \hat{H}_{e\rho}^d$, in which $\hat{H}_{e\rho}^d$ represents the contribution to EPC due to the disorders present in the system (which could be, for example, structural disorder

and is expected to modify the phonon dispersion). After that, Eq. (1.2) can also be expressed as

$$V_{\mathcal{X}\rho} = \langle \mathcal{X} | \hat{H} | \rho \rangle = \langle \mathcal{X} | \hat{H}^0 | \rho \rangle + \langle \mathcal{X} | \hat{H}^d | \rho \rangle = V_{\mathcal{X}\rho}^0 + V_{\mathcal{X}\rho}^d, \quad (1.5)$$

where the terms with superscript d denote, combinedly, the disorder contribution into a system free from disorders denoted by superscript 0.

Further, it is considered that the energy E_ρ of a discrete phonon state would lie in the range of the continuum with values $E_{\mathcal{X}}$. In such a case, an energy value ε within the energy range $E_{\mathcal{X}}$ would be an eigenvalue of the matrix in Eqs. (1.1)–(1.4), and thus, the corresponding eigenvector could be represented as the combination of the states $|\rho\rangle$ and $|\mathcal{X}\rangle$:

$$|\Upsilon\rangle = \alpha |\rho\rangle + \int \beta |\mathcal{X}\rangle dE_{\mathcal{X}}. \quad (2)$$

The integration in the second term runs over the entire energy range of the continuum of the states $|\mathcal{X}\rangle$; α and β depend on ε and can be found as the solutions to the system of Eqs. (1.1)–(1.4). The mathematical steps for the evaluation are provided in Appendix I in the Supplemental Material [79]. The expression for α and β comes out to be

$$\alpha(\varepsilon) = \left\{ \frac{|V_{\varepsilon\rho}^0|^2 + |V_{\varepsilon\rho}^d|^2 + |V_{\varepsilon\rho}^{0*} V_{\mathcal{X}\rho}^d| + |V_{\varepsilon\rho}^{d*} V_{\mathcal{X}\rho}^0|}{[\varepsilon - (E_\rho^0 + E_\rho^d) - F(\varepsilon)]^2 + \pi^2 (|V_{\varepsilon\rho}^0|^2 + |V_{\varepsilon\rho}^d|^2 + |V_{\varepsilon\rho}^{0*} V_{\varepsilon\rho}^d| + |V_{\varepsilon\rho}^{d*} V_{\varepsilon\rho}^0|)^2} \right\}^{1/2}, \quad (3)$$

$$\beta(\varepsilon) = \left\{ \frac{1}{\varepsilon - (E_{\mathcal{X}}^0 + E_{\mathcal{X}}^d)} + \frac{[\varepsilon - (E_\rho^0 + E_\rho^d) - F(\varepsilon)]}{|V_{\varepsilon\rho}^0|^2 + |V_{\varepsilon\rho}^d|^2 + |V_{\varepsilon\rho}^{0*} V_{\varepsilon\rho}^d| + |V_{\varepsilon\rho}^{d*} V_{\varepsilon\rho}^0|} \delta(\varepsilon - E_{\mathcal{X}}) \right\} (V_{\mathcal{X}\rho}^0 + V_{\mathcal{X}\rho}^d) \alpha, \quad (4)$$

where

$$F(\varepsilon) = \text{Principal part of } \int \frac{|V_{\mathcal{X}\rho}^0|^2 + |V_{\mathcal{X}\rho}^d|^2 + |V_{\mathcal{X}\rho}^{0*} V_{\mathcal{X}\rho}^d| + |V_{\mathcal{X}\rho}^{d*} V_{\mathcal{X}\rho}^0|}{\varepsilon - E_{\mathcal{X}}} dE_{\mathcal{X}} \quad (5)$$

represents the shift in position of the resonance energy with respect to E_ρ .

To account the phase shift occurring in the wave function due to interaction between the phononic and electronic states in the presence of disorder, a phase shift parameter θ could be defined, provided the states \mathcal{X} exhibit asymptotic behavior, $|\mathcal{X}\rangle \propto \sin[\mathbf{k}(\varepsilon)\mathbf{r} + \emptyset]$ [55]. Here, $\mathbf{k}(\varepsilon)$ represents the wave vector, \mathbf{r} is the position vector, and \emptyset corresponds to the initial phase. The phase shift parameter θ then would have the form (see Appendix II in the Supplemental Material [79] for the derivation)

$$\theta = -\tan^{-1} \left[\frac{\pi |V_{\varepsilon\rho}^0|^2 + |V_{\varepsilon\rho}^d|^2 + |V_{\varepsilon\rho}^{0*} V_{\varepsilon\rho}^d| + |V_{\varepsilon\rho}^{d*} V_{\varepsilon\rho}^0|}{\varepsilon - (E_\rho^0 + E_\rho^d) - F(\varepsilon)} \right]. \quad (6)$$

Then rewriting α and β from Eqs. (3) and (4):

$$\alpha = \frac{\sin \theta}{\pi V_{\varepsilon\rho}} = \frac{\sin \theta}{\pi (V_{\varepsilon\rho}^0 + V_{\varepsilon\rho}^d)}, \quad (7)$$

$$\begin{aligned} \beta &= \frac{V_{\mathcal{X}\rho}}{\pi V_{\mathcal{X}\rho}^*} \frac{\sin \theta}{\varepsilon - E_{\mathcal{X}}} - \cos \theta \delta(\varepsilon - E_{\mathcal{X}}) \\ &= \frac{(V_{\mathcal{X}\rho}^0 + V_{\mathcal{X}\rho}^d)}{\pi (V_{\varepsilon\rho}^{0*} + V_{\varepsilon\rho}^{d*})} \frac{\sin \theta}{[\varepsilon - (E_{\mathcal{X}}^0 + E_{\mathcal{X}}^d)]} \\ &\quad - \cos \theta \delta[\varepsilon - (E_{\mathcal{X}}^0 + E_{\mathcal{X}}^d)]. \end{aligned} \quad (8)$$

By inclusion of these forms, $|\Upsilon\rangle$ reduces to

$$\begin{aligned} |\Upsilon\rangle &= \frac{\sin \theta}{\pi V_{\varepsilon\rho}} |\rho\rangle \\ &\quad + \int \left[\frac{V_{\mathcal{X}\rho}}{\pi V_{\mathcal{X}\rho}^*} \frac{\sin \theta}{\varepsilon - E_{\mathcal{X}}} - \cos \theta \delta(\varepsilon - E_{\mathcal{X}}) \right] |\mathcal{X}\rangle dE_{\mathcal{X}}. \end{aligned}$$

The role of the phase parameter θ may appear in determining the line shape and its intensity; to account for this, let any phononic excitation occur from some state $|s\rangle$ to state $|\Upsilon\rangle$. The probability of such an excitation may be expressed

through a suitable transition operator \hat{T} (the exact form of \hat{T} is beyond the scope of this paper) for the states as

$$\langle \Upsilon | \hat{T} | s \rangle = \frac{\sin \theta}{\pi V_{\varepsilon \rho}^*} \langle P | \hat{T} | s \rangle - \langle \varkappa | \hat{T} | s \rangle \cos \theta, \quad (9)$$

where

$$|P\rangle = |\rho\rangle + \text{Principal part of } \int \frac{V_{\varkappa \rho} |\varkappa\rangle dE_{\varkappa}}{\varepsilon - E_{\varkappa}}. \quad (10)$$

Equation (10) suggests the modification of the phononic state $|\rho\rangle$ by the states of the continuum. Also, the two terms in Eq. (9) have a phase difference of $\pi/2$, indicating that, as resonance energy is reached ($\theta \rightarrow \pi/2$), the first term dominates, whereas on moving away from this energy value, the terms may interfere destructively on one side, and the transition probability may vanish/diminish, leading to an antiresonance dip in the profile. However, on the other side of resonance energy, the profile could become asymmetric [1,55]. It is noteworthy that, to interfere, the energies corresponding to states $|\rho\rangle$ and $|\varkappa\rangle$ must be comparable, and hence, when the energy difference between the phononic and electronic continuum states is significantly large, such an interaction may not take place. This implies that, for a system free from structural disorder, say at 0 K when the VB is completely occupied, the overlap between electronic and phononic energy states could not be favored. Hence, asymmetry in the Raman line shape due to EPC is not expected at low temperatures. However, the width of Urbach tail states (like electronic disorder) increases with temperature [80]. This could lead to finite overlap of electronic and phononic energy states, from which it could be inferred that the disorders arising in a system may enhance electrophonon interference, which could experimentally reflect as Raman peak broadening, asymmetry, and/or antiresonance diplike features.

Further, to understand the intensity variations due to electron-lattice interactions and disorders, rewriting Eq. (9),

$$\frac{\langle \Upsilon | \hat{T} | s \rangle}{\langle \varkappa | \hat{T} | s \rangle} = \left(\frac{1}{\pi V_{\varepsilon \rho}^*} \frac{\langle P | \hat{T} | s \rangle}{\langle \varkappa | \hat{T} | s \rangle} - \cot \theta \right) \sin \theta. \quad (11)$$

The first term on the right-hand side could be defined as q as done in Ref. [55]:

$$q = \frac{1}{\pi V_{\varepsilon \rho}^*} \frac{\langle P | \hat{T} | s \rangle}{\langle \varkappa | \hat{T} | s \rangle}. \quad (12)$$

Using Eqs. (6) and (12) into Eq. (11), we get

$$\frac{|\langle \Upsilon | \hat{T} | s \rangle|^2}{|\langle \varkappa | \hat{T} | s \rangle|^2} = \frac{(q + \epsilon)^2}{1 + \epsilon^2}, \quad (13)$$

where

$$\begin{aligned} \epsilon = -\cot \theta &= \frac{\varepsilon - E_{\rho} - F(\varepsilon)}{\pi |V_{\varepsilon \rho}|^2}, \\ \epsilon &= \frac{\varepsilon - (E_{\rho}^0 + E_{\rho}^d) - F(\varepsilon)}{\pi (|V_{\varepsilon \rho}^0|^2 + |V_{\varepsilon \rho}^d|^2 + |V_{\varepsilon \rho}^{0*} V_{\varepsilon \rho}^d| + |V_{\varepsilon \rho}^{d*} V_{\varepsilon \rho}^0|)} \\ &= \frac{\varepsilon - E_{\rho} - F(\varepsilon)}{\frac{1}{2}W}, \end{aligned} \quad (14)$$

where $W = 2\pi |V_{\varepsilon \rho}|^2 = 2\pi (|V_{\varepsilon \rho}^0|^2 + |V_{\varepsilon \rho}^d|^2 + |V_{\varepsilon \rho}^{0*} V_{\varepsilon \rho}^d| + |V_{\varepsilon \rho}^{d*} V_{\varepsilon \rho}^0|)$ is the width corresponding to the interaction of the state $|\rho\rangle$ that dilutes throughout a band of states.

In addition, from Eq. (12),

$$\frac{1}{2}\pi q^2 = \frac{1}{W} \frac{|\langle P | \hat{T} | s \rangle|^2}{|\langle \varkappa | \hat{T} | s \rangle|^2}, \quad (15.1)$$

$$q^2 = \frac{1}{\pi^2 (|V_{\varepsilon \rho}^0|^2 + |V_{\varepsilon \rho}^d|^2 + |V_{\varepsilon \rho}^{0*} V_{\varepsilon \rho}^d| + |V_{\varepsilon \rho}^{d*} V_{\varepsilon \rho}^0|)} \frac{|\langle P | \hat{T} | s \rangle|^2}{|\langle \varkappa | \hat{T} | s \rangle|^2}. \quad (15.2)$$

From Eqs. (15.1) and (15.2), parameter $\frac{q^2}{I}$ turns out to be inversely proportional to the width of interaction band W ; here, $I \sim \frac{|\langle P | \hat{T} | s \rangle|^2}{|\langle \varkappa | \hat{T} | s \rangle|^2}$, i.e., the ratio of transition probabilities, which could be related to the intensity of the specific Raman mode as the ratio in the left-hand side of Eq. (13), describes the corresponding line shape, and the term defined as I forms a part of it. In the Eq. (15.2), the term $|V_{\varepsilon \rho}^0|^2$, being the natural width in the absence of any disorder, is considered a constant; the other terms, namely, $|V_{\varepsilon \rho}^d|^2$, $|V_{\varepsilon \rho}^{0*} V_{\varepsilon \rho}^d|$, and $|V_{\varepsilon \rho}^{d*} V_{\varepsilon \rho}^0|$, are the contribution to W due to disorder. Thus, when the disorder grows, the contribution of terms $|V_{\varepsilon \rho}^d|^2$, $|V_{\varepsilon \rho}^{0*} V_{\varepsilon \rho}^d|$, and $|V_{\varepsilon \rho}^{d*} V_{\varepsilon \rho}^0|$ can also increase, and for such a case, the variation in overall width W would significantly depend on the disorder width. It should be noticed that the width W would correspond to the line shape of the profile which could be related to the Raman mode. Further, as these variations are arising due to disorder that may introduce potential fluctuations in the system, the effect of these disorders could be seen as E_u .

It is very important here to note that, for a given semiconductor material, the widths of the Raman phonon mode and the Urbach energy (E_u) show one-to-one correlation [22,65,76,81] as a function of temperature or substitution, or in other words, disorder, i.e., these parameters scale with disorder. Figure 1 shows the linear dependence of E_u with the width of the Raman phonon mode for Hf-substituted BaTiO₃ and TiO₂. The similar one-to-one dependence can also be verified for other samples from the available literature, see Figs. S1–S3 shown in the Supplemental Material [79]. Keeping in view the experimental observation of the linear behavior between the width of the Raman phonon mode and E_u , it is possible to express the width of the Raman peak in terms of E_u as $W = \xi E_u \pm \lambda$, where ξ and λ are material-dependent parameters. Hence, Eq. (15.2) can be rewritten as follows:

$$\frac{1}{2}\pi q^2 = \frac{1}{W} \frac{|\langle P | \hat{T} | s \rangle|^2}{|\langle \varkappa | \hat{T} | s \rangle|^2} = \frac{1}{(\xi E_u \pm \lambda)} \frac{|\langle P | \hat{T} | s \rangle|^2}{|\langle \varkappa | \hat{T} | s \rangle|^2}, \quad (15.3)$$

$$\text{or } \frac{q^2}{I} \propto \frac{1}{(\xi E_u \pm \lambda)}, \quad (15.4)$$

$$\text{or } \frac{I}{q^2} \propto \xi E_u \pm \lambda. \quad (15.5)$$

Therefore, it would be interesting to examine the dependence between the parameter q and E_u . The experimental realization of the same is discussed in subsequent sections.

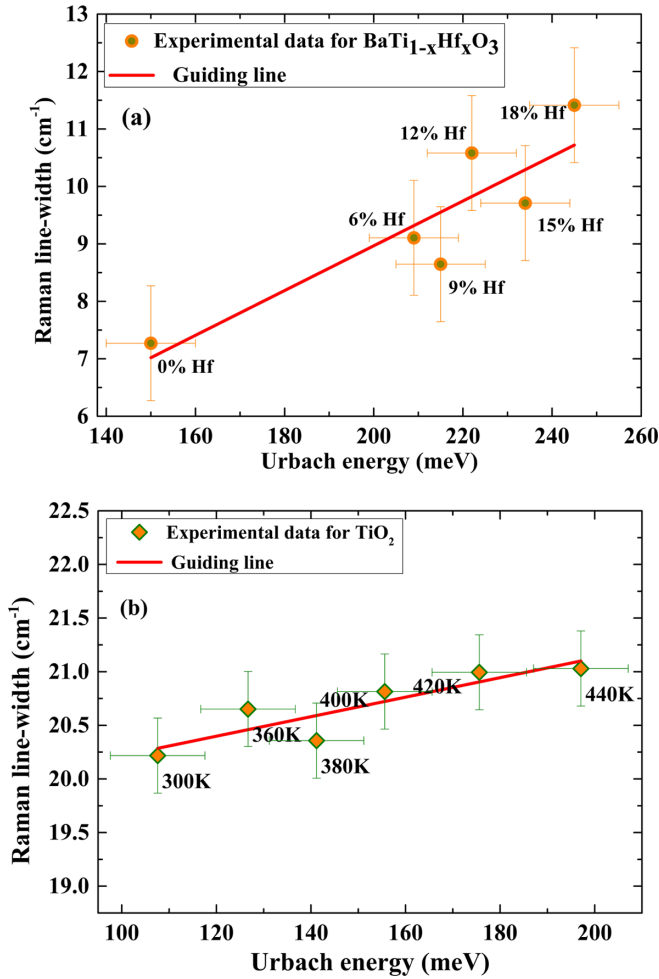


FIG. 1. Linear correlation between the Urbach energy and the Raman linewidth for (a) Hf-substituted BaTiO₃ for Raman mode ~ 300 cm⁻¹ and (b) temperature-varied TiO₂ for Raman mode ~ 515 cm⁻¹.

Now we are in a position to discuss the effect of disorder on the Raman line shape for semiconductor materials. It can be seen from Eq. (3) that the square of the coefficient α has the form of the Lorentzian function of the width $2\pi|V_{\epsilon\rho}|^2$, which can be further expressed as $2\pi(|V_{\epsilon\rho}^0|^2 + |V_{\epsilon\rho}^d|^2 + |V_{\epsilon\rho}^{0*}V_{\epsilon\rho}^d| + |V_{\epsilon\rho}^{d*}V_{\epsilon\rho}^0|)$, implying that, in addition to the natural width $|V_{\epsilon\rho}^0|^2$, the disorder terms also contribute to the overall line width. Mishra *et al.* [82] also reported Raman line broadening due to disorder produced by ion irradiation on MoS₂ layers. Gupta *et al.* [34], in a study on the laser-power-dependent Raman spectrum of Si nanowires, also discussed the effect of thermal disorder as broadening of the Raman mode. Further, the terms $(|V_{\epsilon\rho}^{0*}V_{\epsilon\rho}^d| + |V_{\epsilon\rho}^{d*}V_{\epsilon\rho}^0|)$ may be interpreted as overlapping of the natural and disorder widths, relating to the overlapping of interaction bands corresponding to the natural and disorder introduced states for this paper. It should be noted that Eq. (2) is true only if the energy of the phonon E_ρ lies in the range E_ϵ of the electronic continuum; in that case, the probability of interaction between the states $|\rho\rangle$ and $|\epsilon\rangle$ would increase, which may modify the Lorentzian

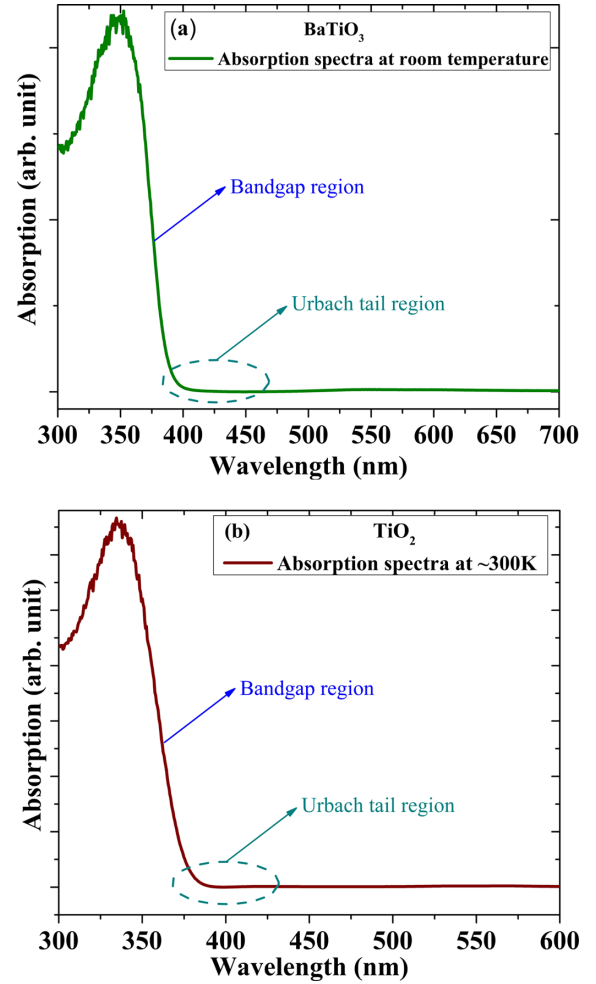


FIG. 2. Schematic representative for the absorption spectra of (a) BaTiO₃ and (b) TiO₂ at room temperature.

line shape of the resonance around the energy value $E_\rho + F(\epsilon)$, leading to asymmetry in the Lorentzian line shape.

Further, the shift in resonance energy is accounted for by the function $F(\epsilon)$ [Eq. (5)], which includes the disorder terms; thus, the presence of disorder could shift the resonance energy. The plot of the quantity in the right-hand side of Eq. (13) vs the reduced energy variable ϵ gives a profile that exhibits asymmetry in the Lorentzian line shape for lower q values that occurs at $\epsilon = 0$ or $\epsilon = E_\rho + F(\epsilon)$, as shown by Fano [55]. The sign and magnitude of parameter q respectively determine the side and extent of asymmetry; hence, q is known as the asymmetry parameter. The line shape is symmetric for higher values of q , whereas as q descends, the line shape first becomes broad, then asymmetric, and a further decrement in q causes an antiresonance dip on the other side of the asymmetry. It is noteworthy here that the ratio of the probability of transition to the state $|\Upsilon\rangle$ to that of the unperturbed states of the continuum $|\epsilon\rangle$ increases with the q value [Eq. (13)]. Also, the line shape height enhances as the q value increases [55]. Thus, it could be inferred that the line intensity would be proportional to the ratio of the transition probabilities in Eq. (13).

Considering Eqs. (15.1)–(15.5), it can be understood that the q value decreases as the disorder width $|V_{\epsilon\rho}^d|^2$ grows,

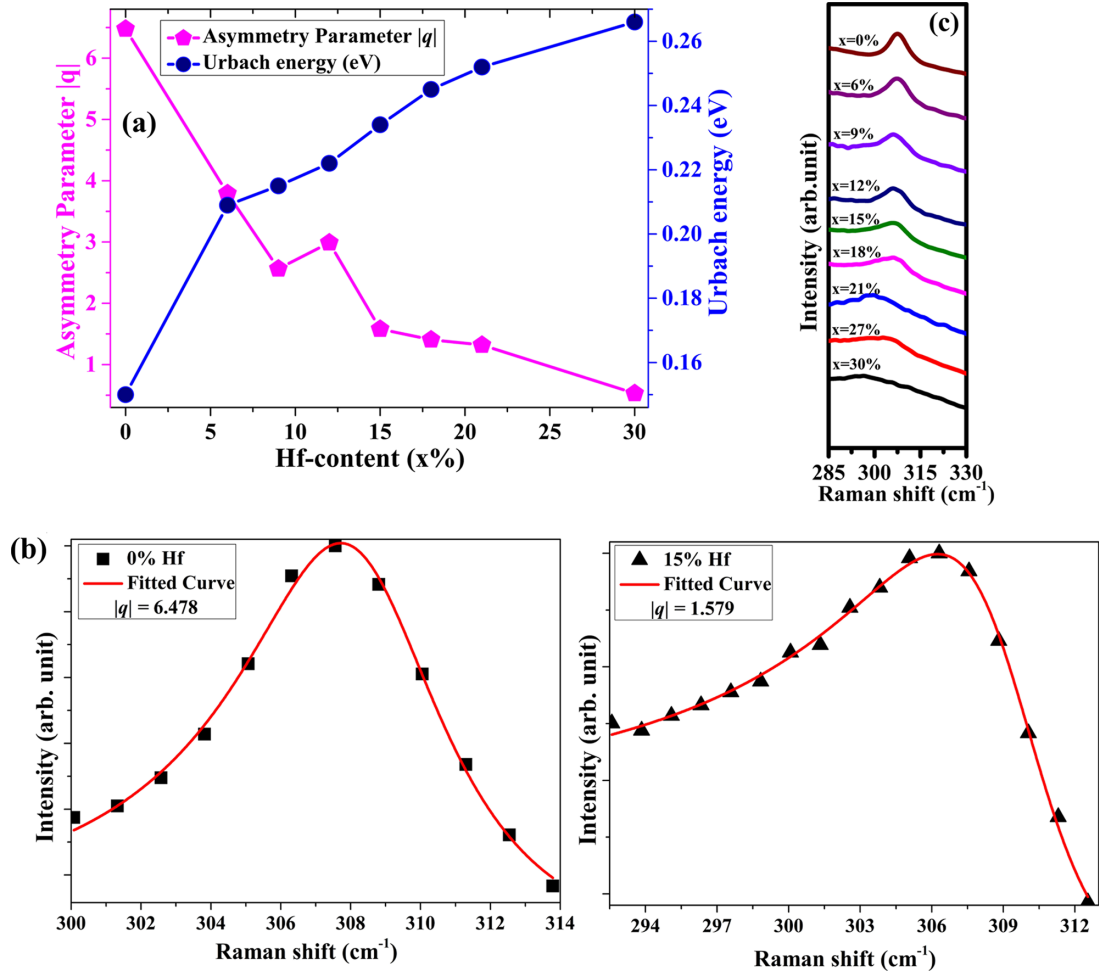


FIG. 3. (a) Plot of asymmetry parameter (q) for the Raman mode ~ 308 cm^{-1} and the Urbach energy (E_u) as a function of Hf-content in $\text{BaTi}_{1-x}\text{Hf}_x\text{O}_3$. (b) Representative figures for fitting of the ~ 308 cm^{-1} Raman mode. (c) The corresponding Raman mode exhibiting increased width and reduced relative intensity with Hf substitution.

suggesting that the corresponding line intensity would reduce [Eq. (13)] with disorder ($\sim |V_{\varepsilon\rho}^d|^2$ terms). The experimental observations reported by Mishra *et al.* [82] also support this interpretation, and the same has also been found in the experimental study in this paper (Supplemental Material [79]). It can be further mathematically elucidated that decrease in the q value may imply either decrease in the ratio of the transition probabilities $\frac{|(P|\hat{T}|s)|^2}{|(\varepsilon|\hat{T}|s)|^2}$ or increase in the width of the interaction band W . Considering the dependence on the width $W \sim |V_{\varepsilon\rho}|^2$, it can be said that, as an extent of interaction, or the overlap between electronic and phononic energies, or W is more, the q value would be less; thus, lower q could indicate stronger electron-lattice interaction, which is experimentally observed in various semiconductors in the form of peak broadening, asymmetry, and/or antiresonance features in Raman spectra [83–85].

IV. EXPERIMENTAL RESULTS AND VALIDATION OF THEORETICAL RELATION

Further, from Eq. (15.2), it can be understood that, for a system with nearly zero disorder, only the term $|V_{\varepsilon\rho}^0|^2$

will contribute to q , and the probability of the interaction $\langle \varepsilon | \hat{T} | s \rangle$ would be negligible (low overlap between electronic and phononic states when disorder is low), which could lead to a relatively very high value of q^2 (ideally infinity) and a highly symmetric Raman mode [Eq. (3)], which is experimentally observed at low temperature for semiconductor materials [81,86,87]. Hence, Eqs. (12) and (15.1)–(15.5) essentially represent a parameter which contains the information of EPC strength.

Now in this section, the validity of the expression in Eq. (15.5) is discussed through experimental data. In this paper, we mainly compare optical and Raman spectroscopic outcomes. The OAS experimentally provides information of the Urbach energy, and Raman spectroscopy provides the information about the asymmetry parameter q . Here, we have carried out two experiments on each of the two different samples. In the first case, disorder has been induced by substituting Hf at the Ti site in the BaTiO_3 system ($\text{BaTi}_{1-x}\text{Hf}_x\text{O}_3$), and in the second case, the disorder is introduced by elevating the temperature of the TiO_2 sample. To check the validity of Eq. (15.4), composition- ($\text{BaTi}_{1-x}\text{Hf}_x\text{O}_3$; BTHO) and temperature- (TiO_2) dependent OAS and Raman spectroscopy measurements were performed. The details on sample

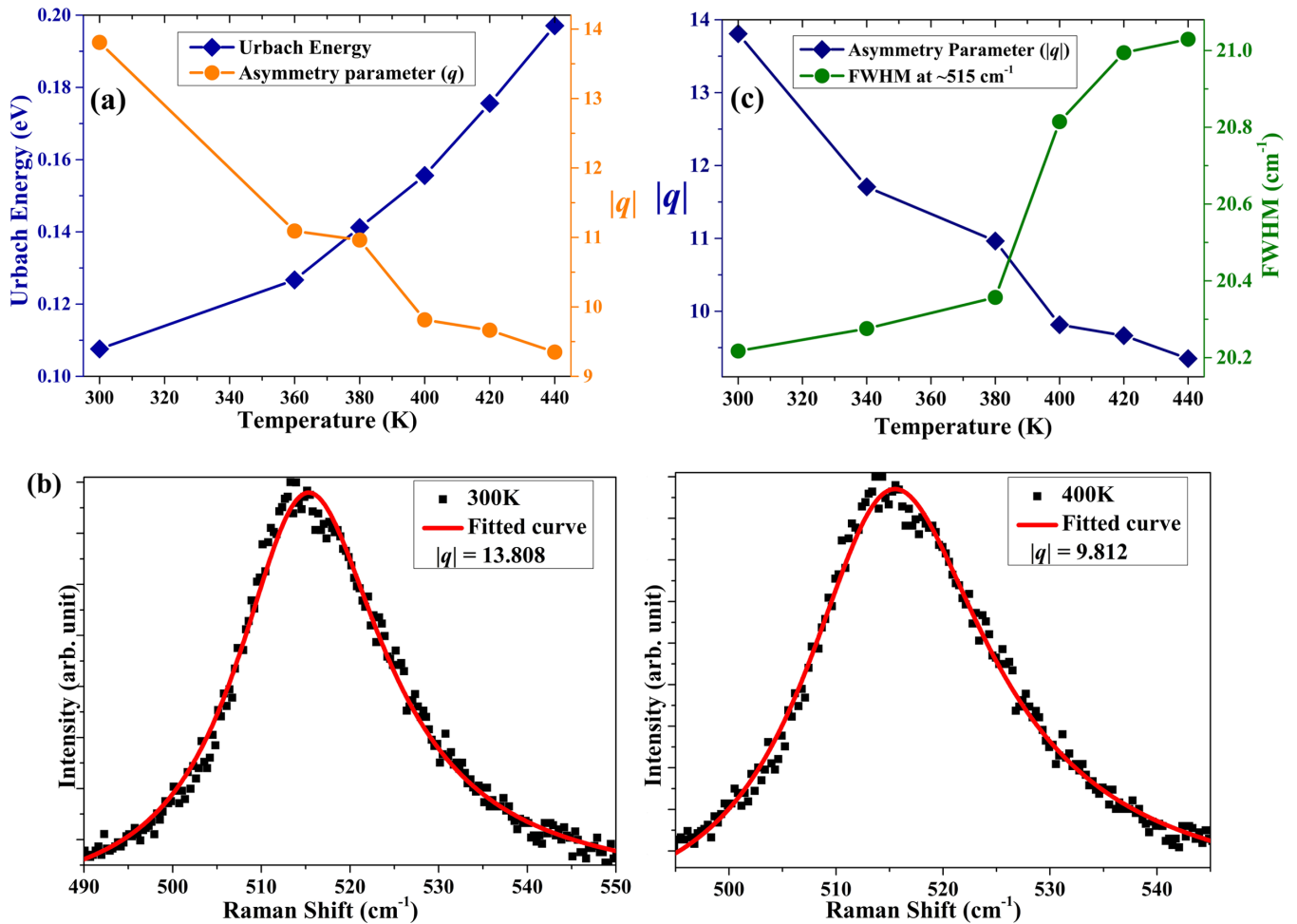


FIG. 4. (a) Temperature dependence of asymmetry parameter (q) corresponding to the $\sim 515 \text{ cm}^{-1}$ Raman mode and the Urbach energy (E_u) for anatase TiO_2 sample. (b) Representative figures for fitting of the $\sim 515 \text{ cm}^{-1}$ Raman mode. (c) Temperature-dependent variation of width of $\sim 515 \text{ cm}^{-1}$ mode and asymmetry parameter.

preparation, estimation of the Urbach energy from the OAS, analysis of Raman spectra, and extraction of the asymmetry parameter q for the phonon mode were provided in earlier publications [25,47,58]. For BTHO samples, OAS were obtained at room temperature (RT); the representatives for the OAS for Hf-substituted BTO and TiO_2 samples at RT are shown in Figs. 2(a) and 2(b), respectively. For BTHO samples, the extracted value of E_u is observed to increase systematically with Hf substitution (Fig. 3). The random distribution of Hf at lattice sites may produce potential fluctuations which may introduce energy levels (Urbach tail states) near the VB/CB that may appear in the form of electronic disorder or E_u [47]. Similarly, for the TiO_2 system, temperature-dependent OAS were recorded [88] to obtain the Urbach energy (E_u). The E_u is found to increase systematically with temperature. It grows from $\sim 107 \text{ meV}$ at 300 K to $\sim 197 \text{ meV}$ at 440 K (Fig. 4), which is consistent with the literature.

Considering the Raman spectra of BTHO samples. The phonon mode assigned to B_1 and $E(\text{TO} + \text{LO})$ that manifests around 308 cm^{-1} in the normalized Raman spectra was studied for the correlation between E_u and the EPC strength, as this mode corresponds to Ti-O bond vibrations [89], which is expected to modify on Hf substitution. The optical and

Raman spectroscopy data reveal that E_u and the FWHM of Raman modes scale with Hf substitution in BaTiO_3 . This mode exhibits enhanced asymmetry with Hf incorporation [Fig. 3(a)]. The increase in the FWHM may be ascribed to the disorder in the phononic energy due to the difference in the ionic radii of Ti^{+4} and Hf^{+4} ions, which results in the larger spread in the phononic states. Hence, the mutual increment of the FWHM and E_u may lead to the overlapping of phononic and electronic energies, providing a favorable condition for the electron-phonon interaction which could appear as asymmetry in the Raman mode [50,53,55]. From Fig. 3(c), it can be seen that the Raman peak $\sim 308 \text{ cm}^{-1}$ broadens systematically accompanied with asymmetry with Hf inclusion, attributing to enhanced EPC in the system. Further, for the purpose of estimating the asymmetry parameter q , the corresponding Raman peak for different compositions has been fitted using the Fano function $I(\omega) = I_0 \frac{(q + \epsilon)^2}{1 + \epsilon^2}$, which is another form of Eq. (13), I_0 being a scaling factor; quantity ϵ , defined as reduced energy variable, is expressed as $\epsilon = (\omega - \omega_0)/\Gamma$, where ω_0 is the frequency (wave number) corresponding to the experimentally observed Raman mode, ω is an independent variable in the frequency (wave number) domain, and Γ is the experimental line width of the Raman

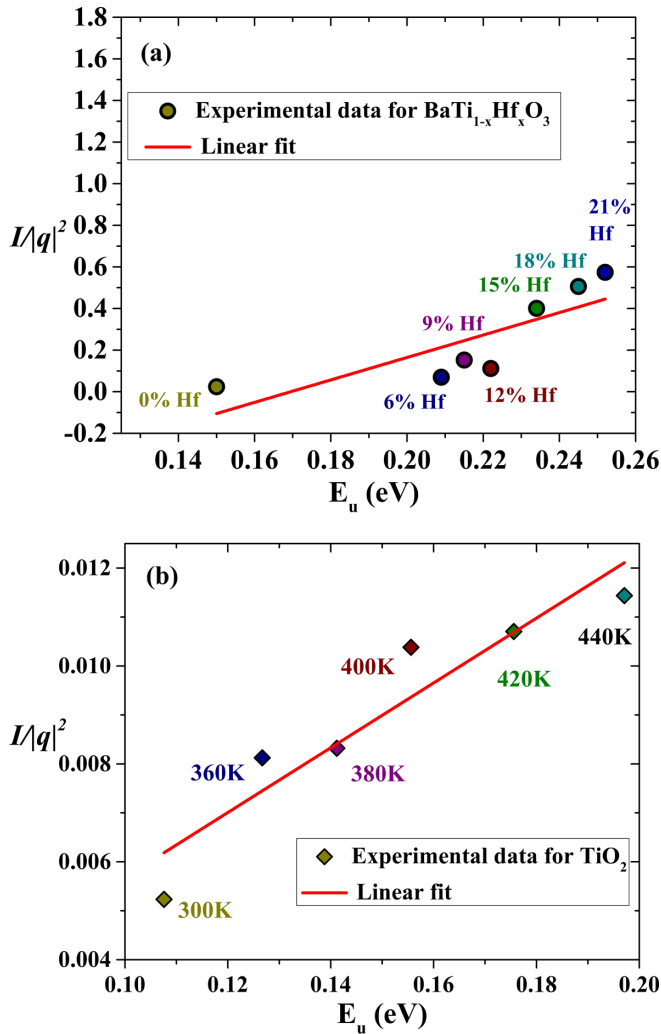


FIG. 5. Plot of I/q^2 vs E_u exhibiting linear dependence for (a) Hf-substituted BaTiO_3 and (b) temperature-varied TiO_2 . See Fig. S7 in the Supplemental Material [79] for similar linear dependence for other phonon modes.

mode; the quantity $I(\omega)$ is proportional to the intensity of the Raman line [47]. The representative schematic for fitted peaks and values of the parameter q obtained for the Raman mode $\sim 308 \text{ cm}^{-1}$ with the Hf content are shown in Figs. 3(a) and 3(b). It is observed that q reduces, whereas E_u scales with Hf substitution, signifying stronger coupling of electrons and phonons with grown disorder. Moreover, for the anatase TiO_2 sample, the $(A_{1g} + B_{1g})$ mode has been found to exhibit enhanced asymmetry among the other phonon modes; therefore, it has been considered for verifying the theoretical outcomes of this paper. Following the similar discussion as for BTHO samples, the corresponding comparisons for the $|q|$ and E_u are shown in Fig. 4. Clearly, the decrease in $|q|$ and scaling of E_u with temperature emphasize the enhancement in EPC due to thermal disorder. The complete measured Raman spectra for BTHO, TiO_2 , and Si single-crystal samples are shown in Figs. S4–S6 in the Supplemental Material [79], respectively.

In this sequence, after qualitatively discussing the correlation between the disorder ($\sim E_u$) and electron-phonon interactions ($\sim 1/q$), we shall now proceed to investigate the

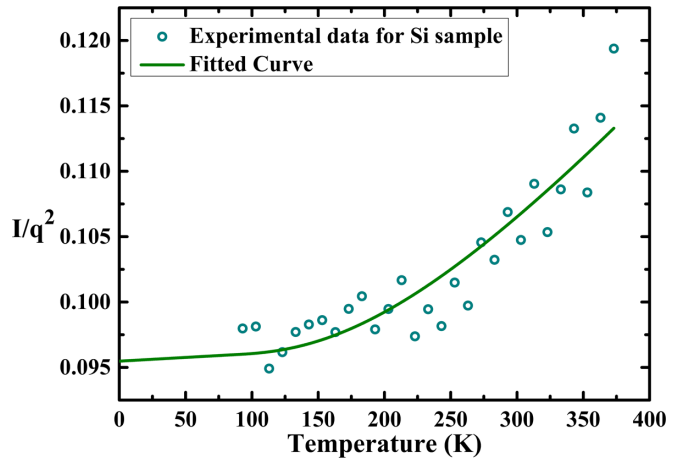


FIG. 6. Temperature-dependent variation of I/q^2 ratio obtained from Raman spectra of single-crystal silicon sample fitted with Einstein single-oscillator model that describes the temperature-dependent variation of the Urbach energy. The variation of experimental data points obtained from Raman spectroscopy is consistent with the fitted theoretical model used for analysis of temperature variation of the Urbach energy.

approached relation in Eq. (15.5). In that regard, Figs. 5(a) and 5(b) show the plot between I/q^2 vs E_u for $\text{BaTi}_{1-x}\text{Hf}_x\text{O}_3$ and TiO_2 systems, respectively. Clearly, the linear trend exhibited by the plot implies that, with increase in disorder in the system, the contribution of disorder terms to the total width W raises, which further contributes to lower q and enhanced EPC. The observed linear behavior is in agreement with the mathematical aspect of Eq. (15.5), demonstrating the increment in the strength of coupling with scaling of E_u which confirms the significant role of E_u (width of the electronic disorder) in the coupling. Nevertheless, the linear plot is found to have some intercept and need not pass through the origin. This offset may be understood as the significance of the parameter λ occurring in Eq. (15.5). There could be three inferences, viz., $\lambda = 0$, $\lambda < 0$, and $\lambda > 0$. In the case of $\lambda > 0$, even though the Urbach energy would tend to zero (origin), the quantity $I/|q|^2$ would still hold some finite value, which may be understood in terms of the intrinsic or characteristic electron-phonon interaction in the material [90]. Moreover, for the cases $\lambda = 0$ and $\lambda < 0$, it may indicate that the system does not possess contribution to the coupling, but disorder may bring it in. Here, for $\lambda < 0$, the negative value of the quantity $I/|q|^2$ would not make sense, as intensity and the square of $|q|$ are positive numbers, and so should be $I/|q|^2$. However, looking at it from another side, it could be seen that, in this case, as E_u approaches zero, i.e., as the system tends to be disorder free, the quantity $I/|q|^2$ would tend toward zero before E_u . This could be inferred as that the system possesses negligible electron-phonon (e -ph) interactions. Hence, a relationship between E_u and EPC in terms of the asymmetry parameter (q) has been explored for correlated systems, which turns out to have the form $I/q^2 \propto E_u \pm \lambda$ that is in agreement with the experimental results. This outcome has also been found consistent with that proposed by Kurik [24].

Furthermore, from the discussion on Eqs. (15.1)–(15.5), it is clear that the ratio I/q^2 would represent a quantity proportional to E_u . To further investigate the correlation of the

ratio I/q^2 and E_u , temperature-dependent Raman spectra of a silicon single crystal has been obtained (see Fig. S3 in the Supplemental Material [79]). A plot between the ratio I/q^2 for the characteristic $\sim 521 \text{ cm}^{-1}$ Raman mode for the silicon sample as function of temperature has been obtained, and shown in Fig. 6. Interestingly, variation of the said ratio as a function of temperature exhibits similar temperature dependence as that of the Urbach energy for silicon [65], in accordance with Einstein's single-oscillator model [65,66], which further confirms the validity of our theoretical model.

V. CONCLUSIONS

In conclusion, our calculations explore the mathematical aspect of disorder-dependent electron-lattice coupling, predicting a correlation between electronic disorder (like Urbach energy, E_u) and coupling-strength ($\sim 1/q$), in semiconductors of the form $I/q^2 \propto E_u$, which has been successfully validated on Hf-substituted BaTiO_3 , temperature-varied TiO_2 , and single-crystal Si with convincing experimental results on three different semiconductors, deducing that electronic disorder has a significant role in determining the coupling in semiconductors. In addition, this model explains mathematically Raman-mode broadening, peak shift, and decrease in its intensity with disorder. Our theoretical results contribute to a deeper insight for understanding the physics of electron-lattice coupling that could be important in tuning the coupling

strength in semiconductors via disorders. This paper brings understanding of EPC in semiconductors with disorder.

ACKNOWLEDGMENTS

All authors sincerely thank the Sophisticated Instrumentation Centre, Indian Institute of Technology (IIT) Indore, for providing characterization facilities. O.V.R. and A.K. acknowledge IIT Indore for providing financial support through Teaching Assistantship. Authors acknowledge the Department of Science and Technology, Science and Engineering Research Board, for financial support through Sanction No. CRG/2018/001829, and Department of Science and Technology, Fund for Improvement of S&T Infrastructure (SR/FST/PSI-225/2016) for providing funding for the Raman spectrometer. Authors acknowledge Dr. Aanchal Sati, Department of Physics, IIT Indore, and Dr. Vikash Mishra, Department of Physics, IIT Bombay, for their valuable participation in experimental data collections. The authors sincerely thank Professor Manavendra Mahato of IIT Indore for fruitful discussions. The authors express gratitude to Professor S. B. Ogale of IISER Pune, Professor Ashok Pimpale of UGC-DAE Consortium for Scientific Research Indore, and Professor Anjali Kshirsager of the Department of Physics, University of Pune, for valuable discussions and comments.

The authors have no competing interest.

-
- [1] F. Bechstedt and K. Peuker, Theory of interference between electronic and phonon Raman scattering, *Phys. Status Solidi B* **72**, 743 (1975).
- [2] D. Dunn, Urbach's rule in an electron-phonon model, *Phys. Rev.* **174**, 855 (1968).
- [3] J. Bardeen, L. N. Cooper, and J. R. Schrieffer, Theory of superconductivity, *Phys. Rev.* **108**, 1175 (1957).
- [4] K. R. Babu and G.-Y. Guo, Electron-phonon coupling, superconductivity, and nontrivial band topology in NbN polytypes, *Phys. Rev. B* **99**, 104508 (2019).
- [5] C. Gadermaier, A. S. Alexandrov, V. V. Kabanov, P. Kusar, T. Mertelj, X. Yao, C. Manzoni, D. Brida, G. Cerullo, and D. Mihailovic, Electron-Phonon Coupling in High-Temperature Cuprate Superconductors Determined from Electron Relaxation Rates, *Phys. Rev. Lett.* **105**, 257001 (2010).
- [6] A. J. Millis, B. I. Shraiman, and R. Mueller, Dynamic Jahn-Teller Effect and Colossal Magnetoresistance in $\text{La}_{1-x}\text{Sr}_x\text{MnO}_3$, *Phys. Rev. Lett.* **77**, 175 (1996).
- [7] P. R. Sagdeo, S. Anwar, and N. P. Lalla, Strain induced coexistence of monoclinic and charge ordered phases in $\text{La}_{1-x}\text{Ca}_x\text{MnO}_3$, *Phys. Rev. B* **74**, 214118 (2006).
- [8] P. R. Sagdeo, N. P. Lalla, A. V. Narlikar, D. Prabhakaran, and A. T. Boothroyd, Strain-induced first-order orbital flip transition and coexistence of charge-orbital ordered phases in $\text{Pr}_{0.5}\text{Ca}_{0.5}\text{MnO}_3$, *Phys. Rev. B* **78**, 174106 (2008).
- [9] J. C. Loudon, S. Cox, A. J. Williams, J. P. Attfield, P. B. Littlewood, P. A. Midgley, and N. D. Mathur, Weak Charge-Lattice Coupling Requires Reinterpretation of Stripes of Charge Order in $\text{La}_{1-x}\text{Ca}_x\text{MnO}_3$, *Phys. Rev. Lett.* **94**, 097202 (2005).
- [10] H. Michor, T. Holubar, C. Dusek, and G. Hilscher, Specific-heat analysis of rare-earth transition-metal borocarbides: An estimation of the electron-phonon coupling strength, *Phys. Rev. B* **52**, 16165 (1995).
- [11] F. Bloch, Über die Quantenmechanik der Elektronen in Kristallgittern, *Z. Für Phys.* **52**, 555 (1929).
- [12] F. Giustino, Electron-phonon interactions from first principles, *Rev. Mod. Phys.* **89**, 015003 (2017).
- [13] L. Nordheim, Zur Elektronentheorie der Metalle. I, *Ann. Phys.* **401**, 607 (1931).
- [14] N. F. Mott and H. Jones, *The Theory of the Properties of Metals and Alloys* (Clarendon Press, Oxford, 1936).
- [15] J. Bardeen, Conductivity of monovalent metals, *Phys. Rev.* **52**, 688 (1937).
- [16] S. Nakajima, in *Proceedings of the International Conference of Theoretical Physics* (Science Council of Japan, Kyoto, Tokyo, 1954).
- [17] J. Bardeen and D. Pines, Electron-phonon interaction in metals, *Phys. Rev.* **99**, 1140 (1955).
- [18] J. P. Carbotte, Properties of boson-exchange superconductors, *Rev. Mod. Phys.* **62**, 1027 (1990).
- [19] J. Bardeen and W. Shockley, Deformation potentials and mobilities in non-polar crystals, *Phys. Rev.* **80**, 72 (1950).
- [20] C. W. Greeff and H. R. Glyde, Anomalous Urbach tail in GaAs, *Phys. Rev. B* **51**, 1778 (1995).
- [21] S. John and M. J. Stephen, Electronic density of states in a long-range correlated potential, *J. Phys. C Solid State Phys.* **17**, L559 (1984).

- [22] J. Huso, H. Che, D. Thapa, A. Canul, M. D. McCluskey, and L. Bergman, Phonon dynamics and Urbach energy studies of MgZnO alloys, *J. Appl. Phys.* **117**, 125702 (2015).
- [23] P. Van Mieghem, Theory of band tails in heavily doped semiconductors, *Rev. Mod. Phys.* **64**, 755 (1992).
- [24] M. V. Kurik, Urbach rule, *Phys. Status Solidi A* **8**, 9 (1971).
- [25] A. Kumar, M. K. Warshi, V. Mishra, S. K. Saxena, R. Kumar, and P. R. Sagdeo, Strain control of Urbach energy in Cr-doped PrFeO₃, *Appl. Phys. A* **123**, 576 (2017).
- [26] G. Gouadec and P. Colombari, Raman spectroscopy of nanomaterials: how spectra relate to disorder, particle size and mechanical properties, *Prog. Cryst. Growth Charact. Mater.* **53**, 1 (2007).
- [27] S. Moser, S. Fatale, P. Krüger, H. Berger, P. Bugnon, A. Magrez, H. Niwa, J. Miyawaki, Y. Harada, and M. Grioni, Electron-Phonon Coupling in the Bulk of Anatase TiO₂ Measured by Resonant Inelastic X-Ray Spectroscopy, *Phys. Rev. Lett.* **115**, 096404 (2015).
- [28] A. H. Castro Neto and F. Guinea, Electron-phonon coupling and Raman spectroscopy in graphene, *Phys. Rev. B* **75**, 045404 (2007).
- [29] J. M. Ziman, *Electrons and Phonons: The Theory of Transport Phenomena in Solids* (Oxford University Press, Oxford, 2001).
- [30] K. Itai, Theory of Raman scattering in coupled electron-phonon systems, *Phys. Rev. B* **45**, 707 (1992).
- [31] J. Bhosale, A. K. Ramdas, A. Burger, A. Muñoz, A. H. Romero, M. Cardona, R. Lauck, and R. K. Kremer, Temperature dependence of band gaps in semiconductors: Electron-phonon interaction, *Phys. Rev. B* **86**, 195208 (2012).
- [32] M. P. Chamberlain, C. Trallero-Giner, and M. Cardona, Theory of one-phonon Raman scattering in semiconductor microcrystallites, *Phys. Rev. B* **51**, 1680 (1995).
- [33] D. Olego and M. Cardona, Self-energy effects of the optical phonons of heavily doped *p*-GaAs and *p*-Ge, *Phys. Rev. B* **23**, 6592 (1981).
- [34] R. Gupta, Q. Xiong, C. K. Adu, U. J. Kim, and P. C. Eklund, Laser-induced Fano resonance scattering in silicon nanowires, *Nano Lett.* **3**, 627 (2003).
- [35] R. N. Jana and A. K. Meikap, Disorder dependence electron phonon scattering rate of V₈₂Pd_{18-x}Fe_x alloys at low temperature, *Phys. Lett. A* **382**, 984 (2018).
- [36] T. Nematirram, A. Asgari, and D. Mayou, Impact of electron-phonon coupling on the quantum yield of photovoltaic devices, *J. Chem. Phys.* **152**, 044109 (2020).
- [37] N. Medvedev and I. Milov, Electron-phonon coupling in metals at high electronic temperatures, *Phys. Rev. B* **102**, 064302 (2020).
- [38] N. Lanatà, Y.-X. Yao, C.-Z. Wang, K.-M. Ho, J. Schmalian, K. Haule, and G. Kotliar, γ - α Isostructural Transition in Cerium, *Phys. Rev. Lett.* **111**, 196801 (2013).
- [39] A. Sergeev, M. Yu. Reizer, and V. Mitin, Deformation Electron-Phonon Coupling in Disordered Semiconductors and Nanostructures, *Phys. Rev. Lett.* **94**, 136602 (2005).
- [40] F. Karsai, M. Engel, E. Flage-Larsen, and G. Kresse, Electron-phonon coupling in semiconductors within the GW approximation, *New J. Phys.* **20**, 123008 (2018).
- [41] G. Benedek, J. R. Manson, and S. Miret-Artés, The electron-phonon interaction of low-dimensional and multi-dimensional materials from He atom scattering, *Adv. Mater.* **32**, 2002072 (2020).
- [42] T. Valla, A. V. Fedorov, P. D. Johnson, and S. L. Hulbert, Many-Body Effects in Angle-Resolved Photoemission: Quasiparticle Energy and Lifetime of a Mo(110) Surface State, *Phys. Rev. Lett.* **83**, 2085 (1999).
- [43] M. X. Na, A. K. Mills, F. Boschini, M. Michiardi, B. Noszarzewski, R. P. Day, E. Razzoli, A. Sheyerman, M. Schneider, G. Levy, S. Zhdanovich, T. P. Devereaux, A. F. Kemper, D. J. Jones, and A. Damascelli, Direct determination of mode-projected electron-phonon coupling in the time domain, *Science* **366**, 1231 (2019).
- [44] Yu. A. Pusep, M. T. O. Silva, J. C. Galzerani, S. W. da Silva, L. M. R. Scolfaro, R. Enderlein, A. A. Quivy, A. P. Lima, and J. R. Leite, Raman study of Fano-like electron-phonon coupling in δ -doping GaAs superlattices, *Phys. Rev. B* **54**, 13927 (1996).
- [45] A. Sunny, A. Thirumurugan, and K. Balasubramanian, Laser induced Fano scattering, electron-phonon coupling, bond length and phonon lifetime changes in α -Fe₂O₃ nanostructures, *Phys. Chem. Chem. Phys.* **22**, 2001 (2020).
- [46] J. Yan, Y. Zhang, P. Kim, and A. Pinczuk, Electric Field Effect Tuning of Electron-Phonon Coupling in Graphene, *Phys. Rev. Lett.* **98**, 166802 (2007).
- [47] A. Sati, V. Mishra, A. Kumar, M. K. Warshi, A. Sagdeo, R. Kumar, and P. R. Sagdeo, Effect of structural disorder on the electronic and phononic properties of Hf doped BaTiO₃, *J. Mater. Sci. Mater. Electron.* **30**, 9498 (2019).
- [48] A. Kumar, S. Umrao, and P. R. Sagdeo, Orbital facilitated charge transfer originated phonon mode in Cr-substituted PrFeO₃: a brief Raman study, *J. Raman Spectrosc.* **51**, 1210 (2020).
- [49] A. Kumar, M. K. Warshi, M. Gupta, and P. R. Sagdeo, The Magneto-elastic and optical properties of multiferroic GaFeO_{3- δ} , *J. Magn. Magn. Mater.* **514**, 167210 (2020).
- [50] A. Sati, A. Kumar, V. Mishra, K. Warshi, P. Pokhriyal, A. Sagdeo, and P. R. Sagdeo, Temperature-dependent dielectric loss in BaTiO₃: Competition between tunnelling probability and electron-phonon interaction, *Mater. Chem. Phys.* **257**, 123792 (2021).
- [51] F. Cerdeira, T. A. Fjeldly, and M. Cardona, Effect of free carriers on zone-center vibrational modes in heavily doped *p*-type Si. II. Optical modes, *Phys. Rev. B* **8**, 4734 (1973).
- [52] Y. G. Wang, S. P. Lau, B. K. Tay, and X. H. Zhang, Resonant Raman scattering studies of Fano-type interference in boron doped diamond, *J. Appl. Phys.* **92**, 7253 (2002).
- [53] M. Gupta, A. Kumar, A. Sagdeo, and P. R. Sagdeo, Doping-induced combined Fano and phonon confinement effect in La-doped CeO₂: Raman spectroscopy analysis, *J. Phys. Chem. C* **125**, 2648 (2021).
- [54] *Light Scattering in Solids IV Electronic Scattering, Spin Effects, SERS, and Morphic Effects*, 1st ed. (Springer Berlin Heidelberg, Berlin, Heidelberg, 1984).
- [55] U. Fano, Effects of configuration interaction on intensities and phase shifts, *Phys. Rev.* **124**, 1866 (1961).
- [56] A. Kumar, A. Sati, V. Mishra, M. K. Warshi, R. Kumar, and P. R. Sagdeo, Charge neutral crystal field transitions: a measure of electron-phonon interaction, *J. Phys. Chem. Solids* **135**, 109102 (2019).

- [57] N. Bouarissa, The effect of compositional disorder on electronic band structure in $\text{Ga}_x\text{In}_{1-x}\text{As}_y\text{Sb}_{1-y}$ alloys lattice matched to GaSb, *Superlattices Microstruct.* **26**, 279 (1999).
- [58] V. Mishra, M. K. Warshi, A. Sati, A. Kumar, V. Mishra, R. Kumar, and P. R. Sagdeo, Investigation of temperature-dependent optical properties of TiO_2 using diffuse reflectance spectroscopy, *SN Appl. Sci.* **1**, 241 (2019).
- [59] F. Cerdeira, A. Pinczuk, J. C. Bean, B. Batlogg, and B. A. Wilson, Raman scattering from $\text{Ge}_x\text{Si}_{1-x}/\text{Si}$ strained-layer superlattices, *Appl. Phys. Lett.* **45**, 1138 (1984).
- [60] E. Anastassakis, A. Pinczuk, E. Burstein, F. H. Pollak, and M. Cardona, Effect of static uniaxial stress on the Raman spectrum of silicon, *Solid State Commun.* **88**, 1053 (1993).
- [61] F. Cerdeira, C. J. Buchenauer, F. H. Pollak, and M. Cardona, Stress-induced shifts of first-order Raman frequencies of diamond- and zinc-blende-type semiconductors, *Phys. Rev. B* **5**, 580 (1972).
- [62] A. Sati, A. Kumar, V. Mishra, K. Warshi, A. Sagdeo, S. Anwar, R. Kumar, and P. R. Sagdeo, Direct correlation between the band gap and dielectric loss in Hf doped BaTiO_3 , *J. Mater. Sci. Mater. Electron.* **30**, 8064 (2019).
- [63] M. Lee, J. Lee, S. Kim, S. Callard, C. Seassal, and H. Jeon, Anderson localizations and photonic band-tail states observed in compositionally disordered platform, *Sci. Adv.* **4**, e1602796 (2018).
- [64] M. Kranjčec, I. P. Studenyak, V. V. Bilanchuk, V. S. Dyordyya, and V. V. Panko, Compositional behaviour of Urbach absorption edge and exciton-phonon interaction parameters in $\text{Cu}_6\text{PS}_5\text{I}_{1-x}\text{Br}_x$ superionic mixed crystals, *J. Phys. Chem. Solids* **65**, 1015 (2004).
- [65] T. Tiedje and J. M. Cebulka, Temperature dependence of the photoconductive absorption edge in amorphous silicon, *Phys. Rev. B* **28**, 7075 (1983).
- [66] M. Ledinsky, T. Schönfeldová, J. Holovský, E. Aydin, Z. Hájková, L. Landová, N. Neyková, A. Fejfar, and S. De Wolf, Temperature dependence of the Urbach energy in lead iodide perovskites, *J. Phys. Chem. Lett.* **10**, 1368 (2019).
- [67] I. Bonalde, E. Medina, M. Rodríguez, S. M. Wasim, G. Marín, C. Rincón, A. Rincón, and C. Torres, Urbach tail, disorder, and localized modes in ternary semiconductors, *Phys. Rev. B* **69**, 195201 (2004).
- [68] K.-I. Noba and Y. Kayanuma, Urbach tail for ferroelectric materials with an order-disorder-type phase transition, *Phys. Rev. B* **60**, 4418 (1999).
- [69] M. K. Warshi, V. Mishra, A. Sagdeo, V. Mishra, R. Kumar, and P. R. Sagdeo, Structural, optical and electronic properties of RFeO_3 , *Ceram. Int.* **44**, 8344 (2018).
- [70] V. Mishra, M. K. Warshi, A. Sati, A. Kumar, V. Mishra, A. Sagdeo, R. Kumar, and P. R. Sagdeo, Diffuse reflectance spectroscopy: An effective tool to probe the defect states in wide band gap semiconducting materials, *Mater. Sci. Semicond. Process.* **86**, 151 (2018).
- [71] A. Kumar, O. V. Rambadey, and P. R. Sagdeo, Unorthodox approach to realize the correlation between the dielectric constant and electronic disorder in Cr-doped PrFeO_3 , *J. Phys. Chem. C* **125**, 7378 (2021).
- [72] A. Kumar, M. K. Warshi, A. Sagdeo, M. Gupta, and P. R. Sagdeo, New route to estimate the Mott-Hubbard and charge transfer parameters: An optical and x-ray absorption studies, *Solid State Sci.* **115**, 106582 (2021).
- [73] V. Mishra, A. Kumar, A. Sagdeo, and P. R. Sagdeo, Comparative structural and optical studies on pellet and powder samples of BaTiO_3 near phase transition temperature, *Ceram. Int.* **46**, 3250 (2020).
- [74] O. V. Rambadey, A. Kumar, A. Sati, and P. R. Sagdeo, Exploring the interrelation between Urbach energy and dielectric constant in Hf-substituted BaTiO_3 , *ACS Omega* **6**, 32231 (2021).
- [75] A. Kumar, M. K. Warshi, A. Sagdeo, M. Krzystyniak, S. Rudić, D. T. Adroja, I. da Silva, and P. R. Sagdeo, Origin of natural and magnetic field induced polar order in orthorhombic $\text{PrFe}_{1/2}\text{Cr}_{1/2}\text{O}_3$, *Phys. Rev. B* **104**, 035101 (2021).
- [76] A. Kumar, V. Mishra, M. K. Warshi, A. Sati, A. Sagdeo, R. Kumar, and P. R. Sagdeo, Strain induced disordered phonon modes in Cr doped PrFeO_3 , *J. Phys. Condens. Matter* **31**, 275602 (2019).
- [77] M. K. Warshi, A. Kumar, A. Sati, S. Thota, K. Mukherjee, A. Sagdeo, and P. R. Sagdeo, Cluster glass behavior in orthorhombic SmFeO_3 perovskite: Interplay between spin ordering and lattice dynamics, *Chem. Mater.* **32**, 1250 (2020).
- [78] D. I. Desnica, M. Kranjčec, and B. Čelustka, Optical absorption edge and Urbach's rule in mixed single crystals of $(\text{Ga}_x\text{In}_{1-x})_2\text{Se}_3$ in the indium rich region, *J. Phys. Chem. Solids* **52**, 915 (1991).
- [79] See Supplemental Material at <http://link.aps.org/supplemental/10.1103/PhysRevB.104.245205> for the appendixes regarding the discussions of this paper and figures of some characterization data.
- [80] J. H. Sun, W. Z. Shen, and F. Y. Meng, Band-tail characteristics in polysilicon, *J. Appl. Phys.* **93**, 9615 (2003).
- [81] T. R. Hart, R. L. Aggarwal, and B. Lax, Temperature dependence of Raman scattering in silicon, *Phys. Rev. B* **1**, 638 (1970).
- [82] P. Mishra, M. Tangi, T. K. Ng, M. N. Hedhili, D. H. Anjum, M. S. Alias, C.-C. Tseng, L.-J. Li, and B. S. Ooi, Impact of N-plasma and Ga-irradiation on MoS_2 layer in molecular beam epitaxy, *Appl. Phys. Lett.* **110**, 012101 (2017).
- [83] M. Chandrasekhar, J. B. Renucci, and M. Cardona, Effects of interband excitations on Raman phonons in heavily doped n -Si, *Phys. Rev. B* **17**, 1623 (1978).
- [84] O. V. Misochko and M. V. Lebedev, Fano interference at the excitation of coherent phonons: Relation between the asymmetry parameter and the initial phase of coherent oscillations, *J. Exp. Theor. Phys.* **120**, 651 (2015).
- [85] I. N. Goncharuk, A. V. Ilinskiy, O. E. Kvashenkina, and E. B. Shadrin, Electron-electron correlations in Raman spectra of VO_2 , *Phys. Solid State* **55**, 164 (2013).
- [86] W. Gebicki, K. Osuch, C. Jastrzebski, Z. Golacki, and M. Godlewski, Raman scattering study of $\text{ZnO}:\text{Ti}$ and $\text{ZnO}:\text{Mn}$ bulk crystals, *Superlattices Microstruct.* **38**, 428 (2005).
- [87] V. Dzhagan, M. Ya. Valakh, J. Kolny-Olesiak, I. Lokteva, and D. R. T. Zahn, Resonant Raman study of phonons in high-quality colloidal CdTe nanoparticles, *Appl. Phys. Lett.* **94**, 243101 (2009).
- [88] V. Mishra, M. K. Warshi, R. Kumar, and P. R. Sagdeo, Design and development of *in-situ* temperature dependent

- diffuse reflectance spectroscopy setup, *J. Instrum.* **13**, T11003 (2018).
- [89] S. Rajan, P. M. M. Gazzali, and G. Chandrasekaran, Impact of Fe on structural modification and room temperature magnetic ordering in BaTiO₃, *Spectrochim. Acta. A* **171**, 80 (2017).
- [90] R. Bhattacharya, R. Mondal, P. Khatua, A. Rudra, E. Kapon, S. Malzer, G. Döhler, B. Pal, and B. Bansal, Measurements of the Electric Field of Zero-Point Optical Phonons in GaAs Quantum Wells Support the Urbach Rule for Zero-Temperature Lifetime Broadening, *Phys. Rev. Lett.* **114**, 047402 (2015).